

Four leptons final states from $\gamma\gamma$ fusion.

Mauro Moretti,
(*e-mail: moretti@vaxfe.fe.infn.it*)

Abstract

I present a systematic study of all possible four leptons final states from $\gamma\gamma$ collisions. It is given a detailed account of fermion masses effects which are sizable since several collinear and t channel enhancements occur. The effects of angular cuts on the final charged leptons are also discussed. To perform the computation I have used the recently developed ALPHA algorithm (and the resulting code) for the automatic computation of scattering amplitudes.

1 Introduction

It appears now technically feasible to operate the future high energy e^+e^- colliders [1] in the $e\gamma$ and $\gamma\gamma$ mode [2]. This last possibility will allow a detailed study of the non abelian nature of the electroweak interactions [3]: triple and quartic gauge boson couplings as well as the coupling of gauge bosons with the higgs particle if it is light enough to be produced.

One of the most important processes to be studied will be W pair production. At high energies, the cross section is dominated by t channel virtual W exchange and becomes nearly constant for a center of mass energy above 400 GeV, with a value of about 90 picobarns. With the aimed luminosity in the range of $10 \div 20$ inverse femtobarns per year about one millions of W pairs are expected.

Since the W boson decays within the detector the experimental signature for W pair production is via its decay products, mostly four fermions in the final state. In view of the forecasted production rate, to address precision studies it is necessary to compute the rate for the process $\gamma\gamma \rightarrow 4 \text{ fermions}$.

In the paper [4], the process $\gamma\gamma \rightarrow \bar{\nu}_e e^- u \bar{d}$ has been studied. In this paper I present a systematic study of leptonic four fermion final states at a $\gamma\gamma$ collider including the effect of fermion masses.

2 The computation

The amplitude for the processes in tables 2, 4 and 6 is computed using a new technique which, in collaboration with *F. Caravaglios* [5], I have recently developed. Exploiting the relation between the one-particle irreducible Green Functions generator Γ and the connected Green Functions generator G we have proposed a simple numerical algorithm to compute tree level scattering amplitudes. We have then implemented the algorithm

$M_W = 80.23 \text{ GeV}$	$\Gamma_W = 2.03367$	$M_Z = 91.1888 \text{ GeV}$	$\Gamma_Z = 2.4974$
$\sin^2 \theta_W = 0.23103$	$\alpha_{QED} = 1./128.07$	$m_e = 0.51 \text{ MeV}$	$m_\mu = 105.66 \text{ MeV}$
$m_\tau = 1.7771 \text{ GeV}$			

Table 1: Input parameters for the electroweak lagrangian. m_e , m_μ , m_τ are the electron muon and tau masses respectively, M_W , M_Z , Γ_W and Γ_Z the W and Z bosons masses and widths, θ_W is the Weinberg angle and α_{QED} is the electromagnetic coupling constant. Tree level relationships among the parameters of the standard model electroweak lagrangian are assumed.

in a FORTRAN code ALPHA which presently uses the standard electroweak lagrangian (QCD is not included yet) and can compute any scattering amplitude in this framework, in a fully automatic way.

The tests we have performed as well as the computations we have done using the ALPHA code are described in the previous papers [4, 5, 6], it is only worth noticing here that, because of the automatic approach to the calculation, there is no need to check the matrix elements for mistakes and bugs.

The input values, which will be used in the present paper, for particles masses, widths and for the electroweak coupling constants are reported in table 1. The gauge bosons propagator π_B is taken as

$$\pi_B^{\mu\nu} = \frac{-i(g^{\mu\nu} - p^\mu p^\nu / M_B^2)}{p^2 - M_B^2 + i\Gamma_B p^2 \theta(p^2) / M_B} \quad (1)$$

where p is the gauge boson four momentum, M_B and Γ_B are the gauge bosons mass and width respectively, and $\theta(p^2)$ is the Riemann θ function: it is equal to one for positive p^2 and zero otherwise.

Although the ALPHA algorithm does not make use of the Feynman graphs technique to compute the scattering matrix elements, it is useful to refer to the Feynman graphs to discuss the main kinematical and dynamical features for the processes under study. The relevant Feynman graphs are given in fig. 1.

The two ¹ diagrams *ra* and *rb* probe the non abelian nature of the Electroweak interactions and involve both triple and quartic gauge bosons self couplings. They describe the production and decay of a pair of on/off shell W. From the form of the propagator of the W boson (1) it is clear that most of the contribution, of the diagrams *ra* and *rb* to the cross section, occurs for almost on shell W. Because of the *t* channel virtual W exchange in the diagram *ra*, for relativistic W, the cross section is strongly peaked for W pairs emitted along the beam direction.

The contribution of the diagram *c* is more important when the internal gauge boson (W, Z or γ) is almost on shell and, for light fermions, when one of the external charged

¹ Actually, in the case of interest here, the diagram *ra* represents *two* diagrams rather than *one*, since, exchanging the two external photon lines, one obtains two inequivalent diagrams. This is essential in doing the computation but does not affect the present discussion. Therefore, in the following, I will not pay attention to the real number of Feynman diagrams but rather to the relevant topologies.

fermions is emitted collinear to the beam direction. In this case, in fact, one of the internal fermions is nearly on shell and this leads to a logarithmic enhancement of the cross section.

The diagram ct has the same ‘singularities’² which have been discussed for the c diagram and has an additional t channel ‘singularity’ when the decaying W boson is emitted collinear to the beam.

The diagram cc exhibits a double collinear ‘singularity’ as well as a t channel virtual gauge boson exchange with the consequent enhancement.

Finally the cf diagram has both a doubly collinear ‘singularity’ as well as the enhancement due to the production of an almost on shell gauge boson.

Due to the large variety of peaking behaviors of the matrix element, to perform the numerical integration over the phase space variables, one needs to increase the sampling in the relevant phase space regions. To this purpose I have used the package VEGAS [7] and all the reported results are obtained with at least twenty VEGAS estimates of the integral with a χ^2 smaller than two. To properly describe the most important phase space regions it has been necessary to split the integration domain into three different regions and to use a suitable set of phase space variables in each of these regions.

The performances of the ALPHA code as an event generator for $\gamma\gamma$ processes are discussed in [4] and will not be repeated here.

3 The results

I will discuss separately the processes which do involve virtual W exchange and which I will call CC (*Charged Current*) processes in the following and those which proceed only via neutral gauge bosons exchange which will be referred as NC (*Charged Current*) processes in the following.

3.1 CC processes

This class of processes can be divided in two additional subclasses: the processes CC_{ee} , $CC_{\mu\mu}$ and $CC_{\tau\tau}$ (see table 2 for the definition of CC_{jk}) where all the final leptons belongs to the same family and the processes $CC_{e\mu}$, $CC_{e\tau}$ and $CC_{\mu\tau}$. The diagrams ra , rb , c , ct and cc do contribute to all CC processes whereas the diagram cf contributes only to single leptonic flavour final states: in this case the virtual gauge boson is a Z boson decaying into a neutrino pair.

The cross section as a function of various angular cuts is plotted in fig. 2 and a few values for some angular cuts are reported in table 2.

The CC_{ee} , $CC_{\mu\mu}$ and $CC_{\tau\tau}$ processes differ among each other only for the mass of the final charged leptons. The effect of fermion masses is manifest. The value of the total (without any cuts) cross section is sensitive to fermion masses, in fact the cross section for the $CC_{\mu\mu}$ and $CC_{\tau\tau}$ processes is lower than that of CC_{ee} process by a factor of about 12% and 17% respectively. The difference is mostly due to the contribution of the diagrams

² Actually the cross sections for the processes I am discussing are finite at the tree level, and the word ‘singularity’ is always used in a loose sense, to denote a small region in the phase space which gives an important contribution to the cross section.

Final State	Label	Energy	$\sigma(0.9)$	$\sigma(0.98)$	$\sigma(0.9975)$	$\sigma(1)$
$e^+e^-\bar{\nu}_e\nu_e$	CC_{ee}	300	0.6537(8)	0.9096(9)	1.001(1)	1.200(2)
$\mu^+\mu^-\bar{\nu}_\mu\nu_\mu$	$CC_{\mu\mu}$	300	0.6533(6)	0.9095(7)	1.0011(8)	1.0767(9)
$\tau^+\tau^-\bar{\nu}_\tau\nu_\tau$	$CC_{\tau\tau}$	300	0.6508(5)	0.9045(5)	0.9921(6)	1.0201(8)
$e^+e^-\bar{\nu}_e\nu_e$	CC_{ee}	500	0.456(1)	0.876(1)	1.091(2)	1.415(2)
$\mu^+\mu^-\bar{\nu}_\mu\nu_\mu$	$CC_{\mu\mu}$	500	0.4555(7)	0.8761(9)	1.090(1)	1.227(1)
$\tau^+\tau^-\bar{\nu}_\tau\nu_\tau$	$CC_{\tau\tau}$	500	0.4536(7)	0.8718(9)	1.083(1)	1.150(1)
$e^+e^-\bar{\nu}_e\nu_e$	CC_{ee}	1000	0.1490(4)	0.545(1)	1.024(2)	1.502(5)
$\mu^+\mu^-\bar{\nu}_\mu\nu_\mu$	$CC_{\mu\mu}$	1000	0.1491(4)	0.5466(9)	1.026(1)	1.313(2)
$\tau^+\tau^-\bar{\nu}_\tau\nu_\tau$	$CC_{\tau\tau}$	1000	0.1486(4)	0.543(1)	1.012(1)	1.191(2)
$e^+\mu^-\bar{\nu}_\mu\nu_e$	$CC_{e\mu}$	300	0.6520(7)	0.9065(8)	0.9958(8)	1.093(1)
$e^+\tau^-\bar{\nu}_\tau\nu_e$	$CC_{e\tau}$	300	0.6509(5)	0.9047(6)	0.9923(6)	1.0689(7)
$\mu^+\tau^-\bar{\nu}_\tau\nu_\mu$	$CC_{\mu\tau}$	300	0.6511(6)	0.9054(7)	0.9928(7)	1.0332(2)
$e^+\mu^-\bar{\nu}_\mu\nu_e$	$CC_{e\mu}$	500	0.4555(6)	0.8754(9)	1.089(1)	1.276(1)
$e^+\tau^-\bar{\nu}_\tau\nu_e$	$CC_{e\tau}$	500	0.4544(5)	0.8733(7)	1.085(1)	1.239(2)
$\mu^+\tau^-\bar{\nu}_\tau\nu_\mu$	$CC_{\mu\tau}$	500	0.4545(4)	0.8733(6)	1.0840(7)	1.1797(9)
$e^+\mu^-\bar{\nu}_\mu\nu_e$	$CC_{e\mu}$	1000	0.1496(4)	0.548(1)	1.024(1)	1.405(2)
$e^+\tau^-\bar{\nu}_\tau\nu_e$	$CC_{e\tau}$	1000	0.1489(3)	0.5450(5)	1.0211(8)	1.339(2)
$\mu^+\tau^-\bar{\nu}_\tau\nu_\mu$	$CC_{\mu\tau}$	1000	0.1491(3)	0.5448(6)	1.0219(8)	1.262(3)
<i>Resonant</i>	Approximation	300	0.6610(3)	0.9073(4)	0.9823(4)	0.9940(4)
<i>Resonant</i>	Approximation	500	0.4770(6)	0.8962(8)	1.0893(8)	1.1244(9)
<i>Resonant</i>	Approximation	1000	0.1671(1)	0.5847(3)	1.0568(4)	1.1923(4)

Table 2: Cross sections for CC processes for center of mass energies of 300, 500 and 1000 GeV. $\sigma(x)$ is the cross section when the angular cut $|\cos\theta_f| < x$ is applied and θ_f is defined as follows: $|\cos\theta_f| = \text{Min}\{|\cos\theta_{l+}|, |\cos\theta_{l-}|\}$ where θ_{l-} and θ_{l+} are the angles of the negatively and positively charged leptons respectively, with the beam direction. Energies are in GeV and cross sections in picobarns.

Energy Cut	$\Delta\sigma_{e\tau}(0.9975)$	$\Delta\sigma_{e\tau}(0.995)$	$\Delta\sigma_{e\tau}(0.99)$	$\Delta\sigma_{e\tau}(0.98)$	$\Delta\sigma_{e\tau}(0.92)$	$\sigma_{ee}(0.9975)$
$E_l > 0$ GeV	7.0(1.2)	5.8(1.2)	4.3(1.2)	3.4(1.1)	1.2(0.9)	1091(1)
$E_l > 3$ GeV	5.3(1.2)	4.3(1.2)	3.0(1.2)	2.4(1.1)	0.73(0.93)	1089(1)
$E_l > 9$ GeV	2.4(1.2)	1.8(1.2)	0.9(1.2)	0.7(1.1)	-0.09(0.9)	1054(1)

Table 3: Difference, in femtobarns, among the cross sections for CC_{ee} and $CC_{\tau\tau}$ processes for a center of mass energy of 500 GeV. E_l is the lowest energy of final charged leptons, $\Delta\sigma_{e\tau}(x)$ is the difference when the angular cut $|\cos\theta_f| < x$ is applied and θ_f is defined as follows: $|\cos\theta_f| = \text{Min}\{|\cos\theta_{l+}|, |\cos\theta_{l-}|\}$ where θ_{l-} and θ_{l+} are the angles of the negatively and positively charged leptons respectively, with the beam direction. σ_{ee} is the cross section for the CC_{ee} process.

c , cc and cf . All these diagrams are divergent, in the limit of massless fermions, when a charged lepton is emitted collinear to the beam. Lepton masses act as a physical cut-off for this collinear logarithmic ‘divergence’ and all the cross sections receive a contribution proportional to $\log(m_l/E_\gamma)$ (m_l is the mass of the relevant lepton). As it can be seen from table 2, if an angular cut is imposed, forcing a small acollinearity with respect to the beam direction for the charged fermions, fermion masses become almost unimportant since the angular cut regulates the ‘divergence’ more efficiently than the lepton masses and the leading contribution of collinearly ‘divergent diagrams’ becomes, irrespectively of the fermion masses, proportional to $\log(1 - \cos\theta_c)$, θ_c being the imposed angular cut.

Even after angular cuts are imposed, a small difference remains among $CC_{\tau\tau}$ and $CC_{\mu\mu}$, CC_{ee} processes. Although, as it can be seen from fig. 2, the accuracy of the computation is not entirely adequate to discuss such a small effect, it appears that the difference is of the order of a few per mille. From purely kinematical considerations one expects an effect of order one per mille: in fact, if one computes the volume of the phase space for the decay of a W boson into a pair of fermions, there is a correction of $m_l^2/(2M_W^2)$ (m_l being the lepton mass) to the result which is obtained assuming massless fermions and, for the τ lepton, this correction is indeed of order one per mille. In table 3 I report a few values of the difference among the cross sections of CC_{ee} and $CC_{\tau\tau}$ processes as a function of several angular and energy cuts. Although, as already noticed, the accuracy of the calculation does not allow a definite conclusion, it seems that the effect disappears when charged fermions energies are greater than $5 \div 10$ GeV and it is slightly weaker when the fermions are emitted at larger angles with respect to the beam. Therefore it seems that, unless a cut of order 10 GeV is imposed on the energies of final leptons, one needs to account also for the dynamical effect of the τ mass.

The $CC_{e\mu}$, $CC_{e\tau}$ and $CC_{\mu\tau}$ processes differ among each other only for the mass of the final charged leptons. They do not receive contribution from the cf diagram and the c diagram is possible only when the internal gauge boson is a W. The cross section as a function of the angular cut is plotted in fig. 3 and some numerical values are reported in tab 2. It is manifest that, with the exception of the already noticed effect of fermion masses in the case of nearly collinear fermion emission, there is no difference, at the per mille level, with single flavour final states. This demonstrates that, when a small angular

Final State	Label	Energy	$\sigma(0.9)$	$\sigma(0.98)$	$\sigma(0.998)$	$\sigma(1)$
$e^+e^-\bar{\nu}_\tau\nu_\tau$	NC_e	300	0.93(1)	2.08(2)	4.57(3)	62.93(8)
$\mu^+\mu^-\bar{\nu}_\tau\nu_\tau$	NC_μ	300	0.943(5)	2.105(8)	4.57(1)	20.89(2)
$\tau^+\tau^-\bar{\nu}_\mu\nu_\mu$	NC_τ	300	0.900(5)	1.979(7)	4.07(1)	7.83(1)
$e^+e^-\bar{\nu}_\tau\nu_\tau$	NC_e	500	0.548(6)	1.9275(9)	2.570(1)	41.41(4)
$\mu^+\mu^-\bar{\nu}_\tau\nu_\tau$	NC_μ	500	0.546(4)	1.191(7)	2.58(1)	14.54(2)
$\tau^+\tau^-\bar{\nu}_\mu\nu_\mu$	NC_τ	500	0.537(3)	1.164(3)	2.441(5)	5.95(1)
$e^+e^-\bar{\nu}_\tau\nu_\tau$	NC_e	1000	0.249(2)	0.508(4)	1.025(6)	18.78(2)
$\mu^+\mu^-\bar{\nu}_\tau\nu_\tau$	NC_μ	1000	0.250(1)	0.512(2)	1.034(3)	7.003(6)
$\tau^+\tau^-\bar{\nu}_\mu\nu_\mu$	NC_τ	1000	0.246(1)	0.507(2)	1.018(2)	3.144(4)

Table 4: Cross sections for NC processes for center of mass energies of 300, 500 and 1000 GeV. Only final states with a neutrino pair. $\sigma(x)$ is the cross section when the angular cut $|\cos\theta_f| < x$ is applied and θ_f is defined as follows: $|\cos\theta_f| = \text{Min}\{|\cos\theta_{l+}|, |\cos\theta_{l-}|\}$ where θ_{l-} and θ_{l+} are the the angles of the negatively and positively charged leptons respectively with the beam direction. Energies are in GeV and cross sections in femtobarns.

cut is applied, the Z exchange contribution (diagrams cf and c) is very small as it can also be seen looking at the rate for the NC_e process (see table 4).

The main contribution to the cross section of CC processes comes from W pair production and decay (diagrams ra and rb in fig. 1). As already discussed in [4] both the narrow width approximation and the approximation (which will be referred as *resonant* approximation in the following) based on the subset of doubly resonant diagrams ra and rb are inadequate for precision studies. In fig. 4 I plot the relative difference among the complete calculation for the CC_{ee} process and the *resonant* approximation: the difference is sizable with any angular cut with the exception of an accidental cancellation at a specific (and energy dependent) value of the angular cut. A few values of the cross section, calculated in the *resonant* approximation, are reported in table 2. The discrepancy increases with the beam energy and this corroborates the hypothesis that the effect is due to the lack of gauge invariance of the *resonant* approximation and to the related unitarity violation.

3.2 NC processes

Let us first discuss those processes involving a final neutrino pair NC_e , NC_μ and NC_τ . They all proceed via virtual, on/off shell, Z boson exchange (diagrams c and cf). The cross section is plotted in fig. 5 as a function of the angular cut and a few values are reported in table 4. There is again a significative effect of fermion masses for fermion emission at very small angles with respect to the beam direction and the difference disappears for acollinear fermions. The size of the cross sections for these processes provides an indirect confirmation of the observation made for CC processes for which Z exchange contribution appears to be negligible at the level of accuracy of the present computation.

The production of four charged leptons proceeds via the exchange of virtual on/off

Energy Cut	$\sigma(\alpha_3, \beta_2)$	$\sigma(\alpha_3, \beta_1)$	$\sigma(\alpha_2, \beta_2)$	$\sigma(\alpha_2, \beta_1)$	$\sigma(\alpha_1, \beta_2)$	$\sigma(\alpha_1, \beta_1)$
$E_l > 0$ GeV	4.08(11)	4.70(12)	8.29(22)	9.74 (23)	136(1)	661(2)
$E_l > 2$ GeV	4.07(11)	4.70(12)	8.28(22)	9.74 (22)	136(1)	660(2)
$E_l > 4$ GeV	3.99(11)	4.60(12)	8.13(22)	9.57 (22)	132(1)	649(2)
$E_l > 6$ GeV	3.84(10)	4.45(12)	7.90(22)	9.32 (22)	127(1)	633(2)
$E_l > 9$ GeV	3.68 (10)	4.27(12)	7.59(21)	8.97(22)	119(1)	605(2)

Table 5: Cross sections for $NC_{\tau\tau}$ process for a center of mass energies of 500 GeV. $\sigma(x_1, x_2)$ is the cross section when the angular cuts $|\cos\theta_f| < x_1$ $|\cos\theta_p| < x_2$ are applied and θ_f, θ_p are defined as follows: $|\cos\theta_f| = \text{Min}\{|\cos\theta_j|\}$ and $|\cos\theta_p| = \text{Min}\{\cos\theta_{j,k}\}$ where θ_j are the the angles of the charged leptons with the beam direction and $\theta_{j,k}$ are the angles among each final lepton pairs. The angles $\alpha_1, \alpha_2, \alpha_3, \beta_1$ and β_2 are equal to $0^\circ, 5.89^\circ, 8.61^\circ, 0^\circ$ and 8.33° degrees respectively and E_l is the lowest among final leptons energies. Cross sections are in femtobarns.

shell Z bosons and photons (diagrams c, cf and cc). When no cut is applied on the final leptons the cross section is dominated by the t channel virtual photon exchange of diagram cc . This diagram is singular if the virtual photon become massless and the only cut-off to this ‘singularity’ is provided by the fermion masses. The expected behavior of the cross section is therefore $\sigma \sim 1/m_f^2$ times the logarithmic enancement due to the collinear ‘singularities’ associated with internal fermions lines. Especially for $e^+e^-e^+e^-$ final state the cross section is huge. In table 5 I give a few values of the cross section for the $\tau^+\tau^-\tau^+\tau^-$ final state as a function of various angular cuts. As expected most of the cross section occurs for final leptons collinear to the beam and very close (in direction) to each other.

Since the detection unavoidably will discard such events in table 6 I report the cross sections for this class of processes imposing the requirement that final leptons are emitted with an angle of at least 2° with respect to the beam direction and among each other. Although this requirements appears extremely mild the effect is manifest: the cross section is drastically reduced since now the cut-off on the internal photons virtuality is much harder. In fig. 6 I plot the cross section for the NC_{ee} process as a function of various angular cuts.

Lepton energies are also relevant and there is a sizable production of low energy leptons. In fact although disfavored because of the small phase space these events are enanced because lepton pairs with low invariant mass and momentum are produced. In table 7 the cross section as a function of several angular and energy cuts is reported for the process $NC_{e\mu}$.

4 Conclusions

I have used the recently developed ALPHA algorithm (and the resulting code) to perform a systematic study of the processes $\gamma\gamma \rightarrow 4 \text{ leptons}$ which will be relevant at future e^+e^-

Final State	Label	Energy	$\sigma(\alpha_2, \beta_2)$	$\sigma(\alpha_2, \beta_1)$	$\sigma(\alpha_1, \beta_2)$	$\sigma(\alpha_1, \beta_1)$
$e^+e^-e^+e^-$	NC_{ee}	300	15.89(46)	34.2(5.7)	275(3)	1174(8)
$\mu^+\mu^-\mu^+\mu^-$	$NC_{\mu\mu}$	300	13.25(23)	18.93(80)	266(3)	1078(6)
$\tau^+\tau^-\tau^+\tau^-$	$NC_{\tau\tau}$	300	9.89(42)	11.04(43)	145(1)	320(2)
$e^+e^-\mu^+\mu^-$	$NC_{e\mu}$	300	30.8(6)	48.1(1.0)	535(4)	2292(23)
$e^+e^-\tau^+\tau^-$	$NC_{e\tau}$	300	28.7(1.0)	42.0(1.3)	402(4)	1215(5)
$\mu^+\mu^-\tau^+\tau^-$	$NC_{\mu\tau}$	300	24.2(8)	29.1(8)	384(2)	1145(3)
$e^+e^-e^+e^-$	NC_{ee}	500	6.13(33)	9.68(71)	99.46(88)	412(2)
$\mu^+\mu^-\mu^+\mu^-$	$NC_{\mu\mu}$	500	5.69(21)	8.28(82)	97.7(7)	411(2)
$\tau^+\tau^-\tau^+\tau^-$	$NC_{\tau\tau}$	500	4.16(12)	4.69(12)	68.39(93)	188(1)
$e^+e^-\mu^+\mu^-$	$NC_{e\mu}$	500	12.28(40)	18.9(1.4)	200(2)	834.0(3)
$e^+e^-\tau^+\tau^-$	$NC_{e\tau}$	500	11.2(5)	16.2(8)	168(3)	576.2(3)
$\mu^+\mu^-\tau^+\tau^-$	$NC_{\mu\tau}$	500	9.04(21)	10.7(2)	166(4)	555(5)
$e^+e^-e^+e^-$	NC_{ee}	1000	1.57(7)	2.55(37)	27.33(94)	110(1)
$\mu^+\mu^-\mu^+\mu^-$	$NC_{\mu\mu}$	1000	1.56(11)	2.04(11)	25.22(29)	102.6(6)
$\tau^+\tau^-\tau^+\tau^-$	$NC_{\tau\tau}$	1000	1.42(11)	1.62(11)	20.87(18)	69.8(2)
$e^+e^-\mu^+\mu^-$	$NC_{e\mu}$	1000	3.36(16)	4.76(18)	50.70(78)	215.6(3.6)
$e^+e^-\tau^+\tau^-$	$NC_{e\tau}$	1000	3.20(13)	4.57(25)	48.8(1.6)	178.0(1.7)
$\mu^+\mu^-\tau^+\tau^-$	$NC_{\mu\tau}$	1000	3.04(15)	3.81(17)	47.0(8)	173.0(1.0)

Table 6: Cross sections for NC processes for center of mass energies of 300, 500 and 1000 GeV. Only final states with four charged leptons in the final state. $\sigma(x_1, x_2)$ is the cross section when the angular cuts $|\cos\theta_f| < x_1$ $|\cos\theta_p| < x_2$ are applied and θ_f , θ_p are defined as follows: $|\cos\theta_f| = \text{Min}\{|\cos\theta_j|\}$ and $\cos\theta_p = \text{Min}\{\cos\theta_{j,k}\}$ where θ_j are the the angles of the charged leptons with the beam direction and $\theta_{j,k}$ are the angles among each final lepton pairs. The angles α_1 , α_2 , β_1 and β_2 are equal to 2° , 8.61° , 2° and 8.33° degrees respectively. Energies are in GeV and cross sections in femtobarns.

Energy	Energy Cut	$\sigma(\alpha_2, \beta_2)$	$\sigma(\alpha_2, \beta_1)$	$\sigma(\alpha_1, \beta_2)$	$\sigma(\alpha_1, \beta_1)$
300	$E_l > 0$ GeV	30.83(60)	48.1(1.0)	535(4)	2292(23)
300	$E_l > 3$ GeV	21.92(44)	30.47(68)	463(4)	2028(14)
300	$E_l > 9$ GeV	17.09(43)	22.58(65)	361(4)	1619(14)
500	$E_l > 0$ GeV	12.25(40)	18.9(1.4)	200(2)	834(3)
500	$E_l > 3$ GeV	9.56(28)	14.9(1.4)	182(2)	778(3)
500	$E_l > 9$ GeV	8.06(27)	10.7(3)	156(2)	675(3)
1000	$E_l > 0$ GeV	3.36(16)	4.76(18)	50.70(78)	216(4)
1000	$E_l > 3$ GeV	3.00(16)	4.08(17)	47.48(63)	207(4)
1000	$E_l > 9$ GeV	2.62(15)	3.44(15)	43.71(62)	193(4)

Table 7: Cross sections for $NC_{e\mu}$ process for center of mass energies of 300, 500 and 1000 GeV. $\sigma(x_1, x_2)$ is the cross section when the angular cuts $|\cos \theta_f| < x_1$ $|\cos \theta_p| < x_2$ are applied and θ_f , θ_p are defined as follows: $|\cos \theta_f| = \text{Min}\{|\cos \theta_j|\}$ and $|\cos \theta_p| = \text{Min}\{|\cos \theta_{j,k}|\}$ where θ_j are the angles of the charged leptons with the beam direction and $\theta_{j,k}$ are the angles among each final lepton pairs. The angles α_1 , α_2 , β_1 and β_2 are equal to 2° , 8.61° , 2° and 8.33° degrees respectively, E_l is the lowest among final leptons energies. Energies are in GeV and cross sections in femtobarns.

colliders when operating in the $\gamma\gamma$ mode.

For those process which proceed via virtual W exchange (labelled as CC_{jk} in the text and in table 2) the bulk of the cross section is due to the production and decay of a W pair. Another important contribution, at the level of several per cent, arises because of the emission of a collinear fermion and a single W. To perform precision studies the full computation is therefore needed.

When no angular cut is imposed fermion masses act as cut-off of the singularities which occur in correspondence of charged fermions emitted collinear to the beam direction and are therefore relevant. If a moderate angular cut is imposed fermion masses become almost unimportant.

Because of the contribution of t channel virtual W exchange of the diagram *ra* the total rate is nearly constant for a center of mass energy above 400 GeV. When angular cuts are imposed the usual fall-off with the center of mass energy is observed.

The reactions which proceed only via neutral gauge bosons exchange (labelled NC_{jk} in the text and in tables 4 and 6) present different features according to the charge multiplicity of the final state.

If in the final state there are a neutrino and a charged lepton pairs the bulk of the cross section is due to the *c* diagram when both of the charged fermions are collinear to the beam a Z boson is emitted and then decay in a neutrino pair. The cross section is always below a few femtobarns with the exception of fermions emitted very close to the beam direction where fermion mass effects are important and the cross sections range from a few to one hundred femtobarns

If in the final state there are two pairs of charged fermions the bulk of the contribution comes from the diagram cc , namely the two photon radiates a pair of almost on shell fermions and two of these fermions undergo compton scattering with its characteristic singularity in the forward direction. Since the fermions which scatter have a small virtuality the typical rate of these processes is proportional to $1/m_l^2$ times logarithmic enhancements. Because of the smallness of lepton masses the resulting cross sections are huge and strongly dependent on angular cuts: a relatively mild angular cut is enough to reduce the rate by order of magnitudes.

A final comment is in order here: because of the finite (and *running* width of massive gauge bosons in (1) the results I have presented are not gauge invariant. A discussion (incomplete) about this issue can be found in [4] where it is argued that it is likely that this fact is numerically irrelevant (in the Unitary gauge which is used here). This fact has anyway to be confirmed by an explicit computation which must respect gauge invariance as well as account for gauge bosons widths in a satisfactory way.

Acknowledgments

I thank the *Associazione per lo Sviluppo della Fisica Subatomica, Ferrara* for financial support and *INFN, sezione di Ferrara* for making available computing facilities.

References

- [1] *Proceedings of the Workshop on e^+e^- Collisions at 500 GeV: The Physics Potential*, DESY 92-123B, Ed. P. Zerwas.
- [2] I. F. Ginzburg *et al.*, Nucl. Phys. B228 (1983) 285; Nucl. Instrum. Methods 205 (1984) 47.
- [3] M. Baillargeon and F. Boudjema, Phys. Lett. B317 (1993) 371; G.J. Gounnaris, J. Layssac and F.M. Reynard Z. Phys. C 69 (1996) 505.
- [4] M. Moretti, *Four Fermions Production at a $\gamma\gamma$ collider*, hep-ph 9604303, *preprint*
- [5] F. Caravaglios and M. Moretti, Phys. Lett. B358(1995)332; *e^+e^- into four fermions plus γ with ALPHA*, OUTP 9613 P, *preprint*.
- [6] D. Bardin, R. Kleiss *et. al.*, *Event Generators for WW Physics on Proceedings of The LEP200 Workshop*, Cern Report (1995).
- [7] G. P. Lepage, J. Comput. Phys. 27 (1978) 192.

Figure Captions

- Fig. 1 Feynman diagrams for $\gamma\gamma \rightarrow 4 \text{ fermions}$. Straight lines represents fermions and wiggled lines gauge bosons.
- Fig. 2 Cross section for CC_{jj} processes as a function of the angular cut θ_f . The processes are listed in table 2 and the definition of the angle θ_f is given in the caption of the same table. σ_{jj} is the cross section for the CC_{jj} process and $\Delta\sigma_{jk} = (\sigma_{kk} - \sigma_{jj})/\sigma_{jj}$. Continuous and dashed line refer to the value of $\Delta\sigma_{jk}$ plus and minus one standard deviation respectively.
- Fig. 3 Cross section for the $CC_{e\mu}$ processes as a function of the angular cut θ_f . The processes are listed in table 2 and the definition of the angle θ_f is given in the caption of the same table. $\sigma_{e\mu}$ is the cross section for the CC_{jj} process and $\Delta\sigma = (\sigma_{ee} - \sigma_{e\mu})/\sigma_{ee}$. E_{CM} is the total energy in the center of mass. Continuous and dashed line refer to the value of $\Delta\sigma$ plus and minus one standard deviation respectively.
- Fig. 4 Relative difference among the full calculation and the resonant approximation for the cross section of the CC_{ee} processes as a function of the angular cut θ_f . The processes are listed in table 2 and the definition of the angle θ_f is given in the caption of the same table. $\Delta\sigma = (\sigma_{ee} - \sigma_{resonant})/\sigma_{ee}$. E_{CM} is the total energy in the center of mass. The resonant approximation amounts to consider only the diagrams *ra* and *rb* in fig. 1. Continuous and dashed line refer to the value of $\Delta\sigma$ plus and minus one standard deviation respectively.
- Fig. 5 Cross section in femtobarns for the NC_e process at a center of mass energies of 300, 500 and 1000 GeV as a function of the angular cut θ_f . E_{CM} is the center of mass energy and the definition of θ_f is given in the caption of table 4.
- Fig. 6 Cross section in femtobarns for the $NC_{e\mu}$ process at a center of mass energy of 500 GeV as a function of the angular cut θ_f (θ_p) at fixed values of the angular cut θ_p (θ_f). The definitions of θ_p and θ_f are given in the caption of table 6.

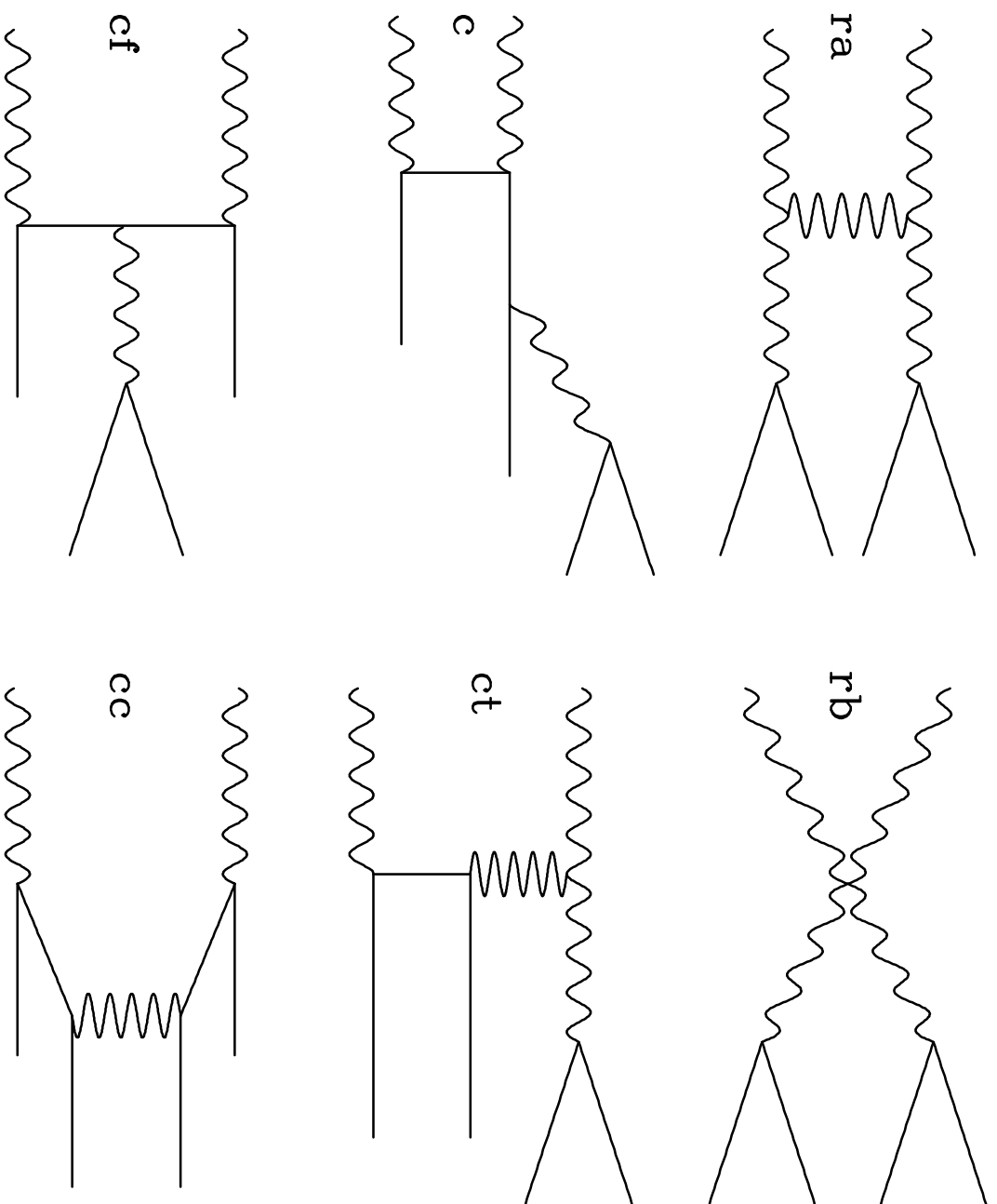


Fig. 1

$\cos\theta_f$

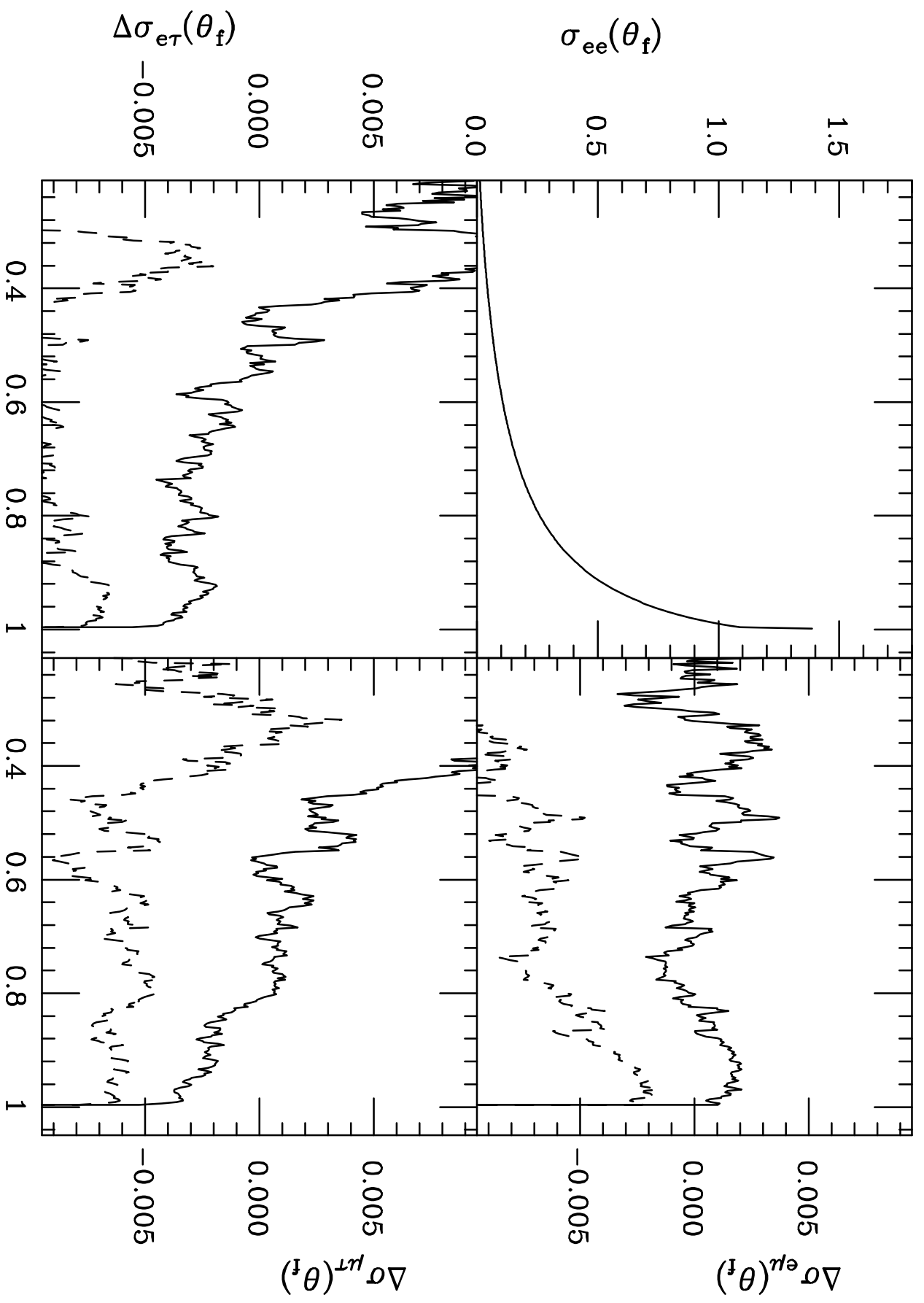


Fig. 2

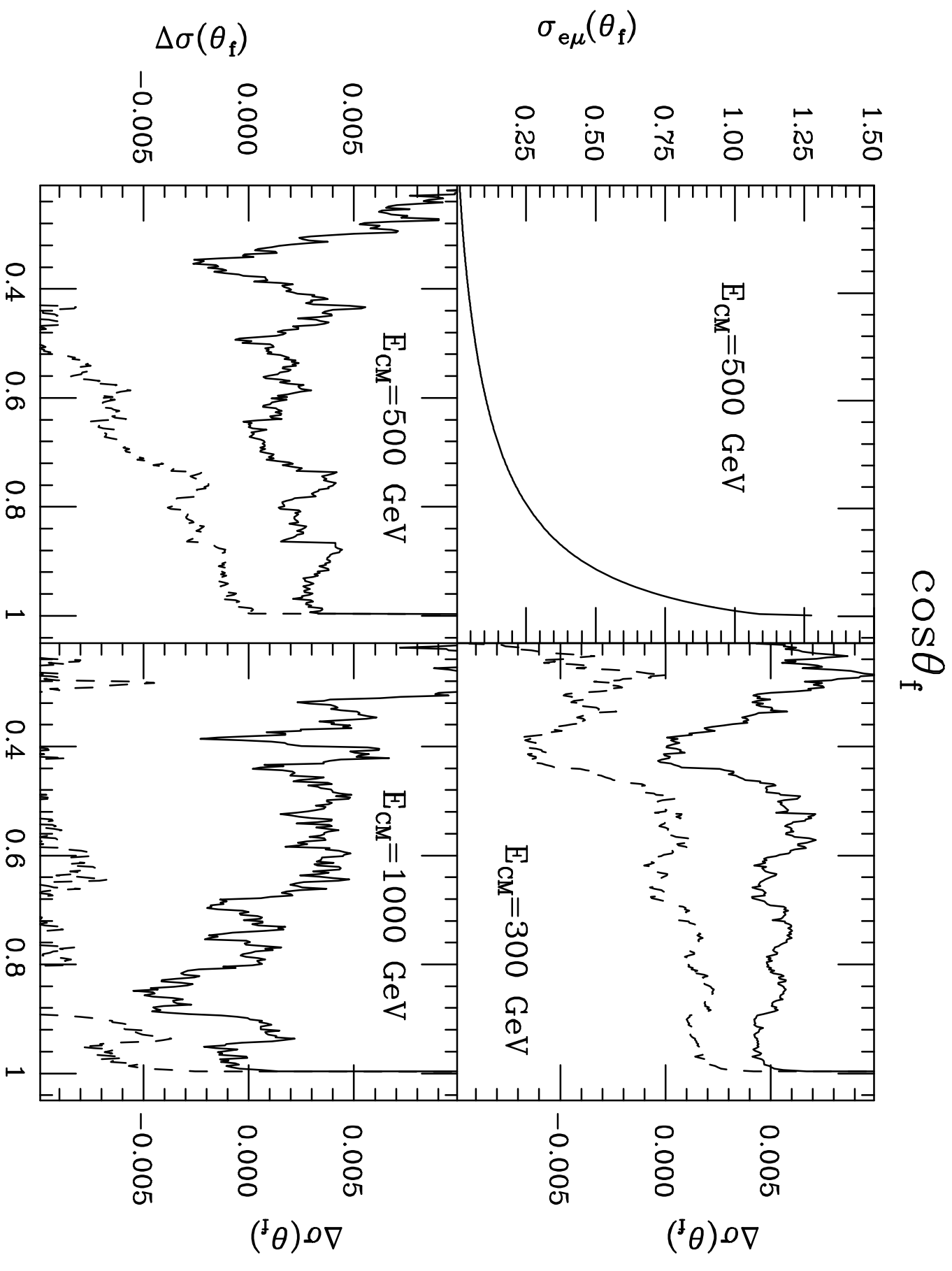


Fig. 3

$\cos\theta_f$

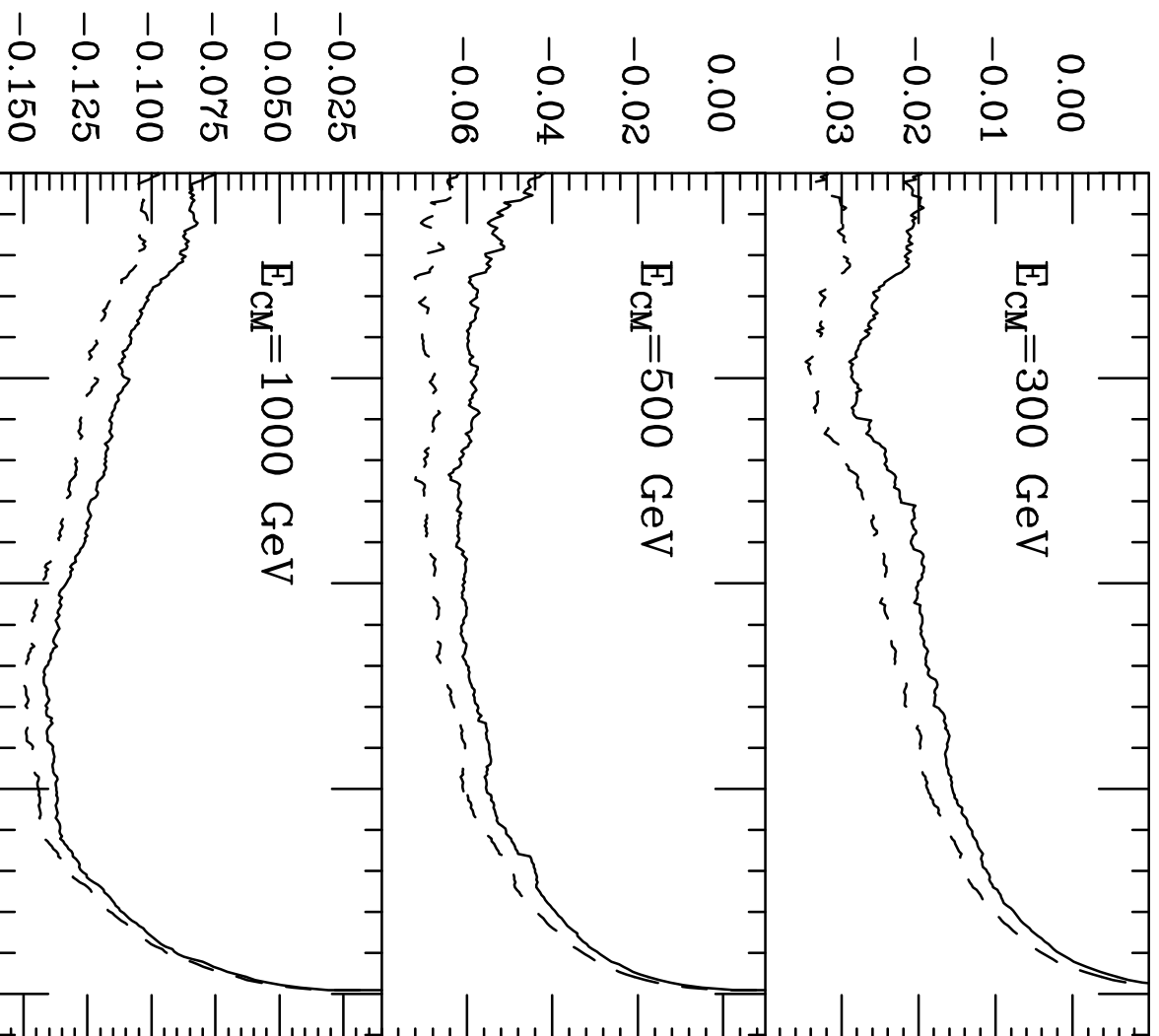


Fig. 4

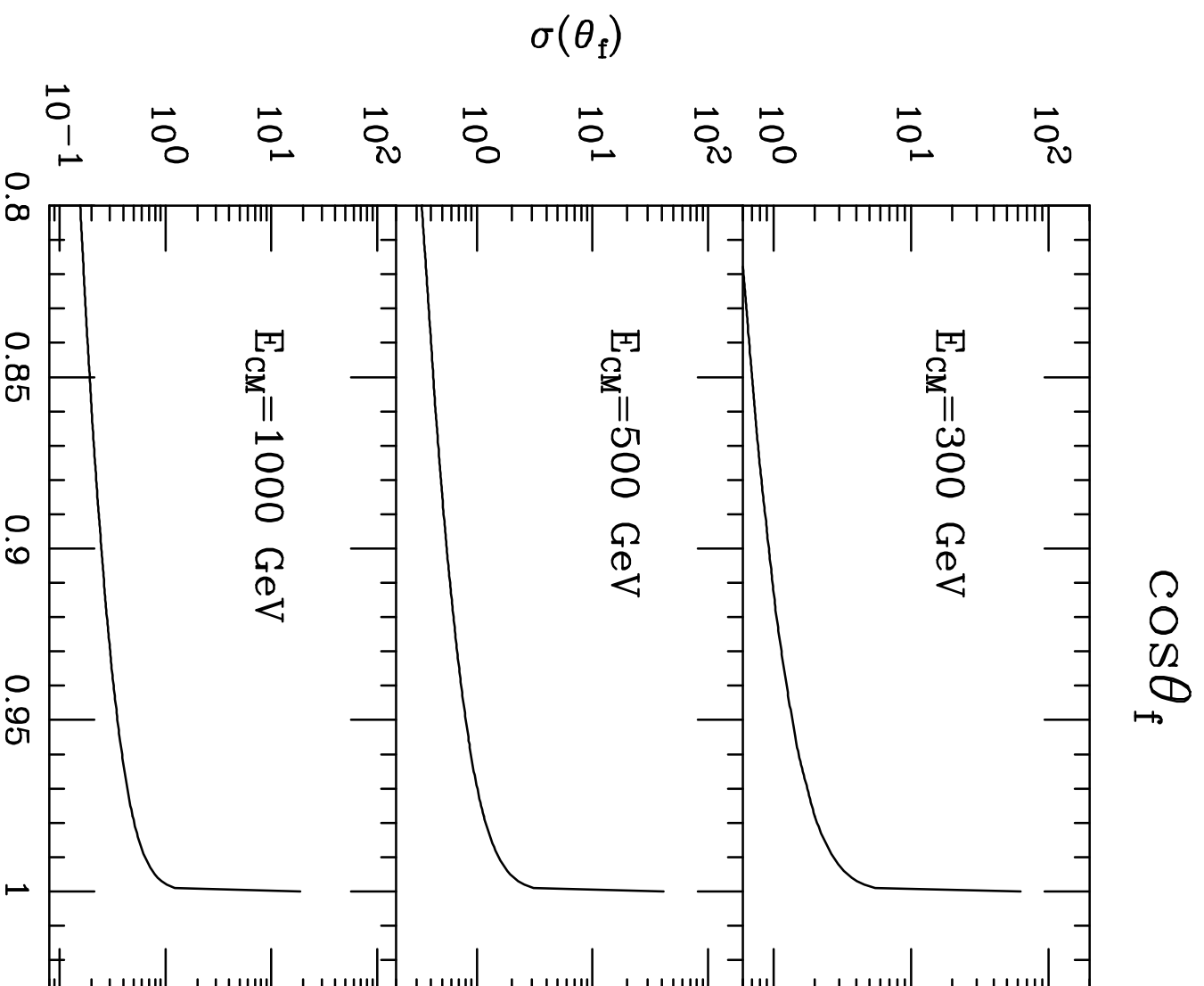


Fig. 5

$\cos\theta_f$

$\cos\theta_p$

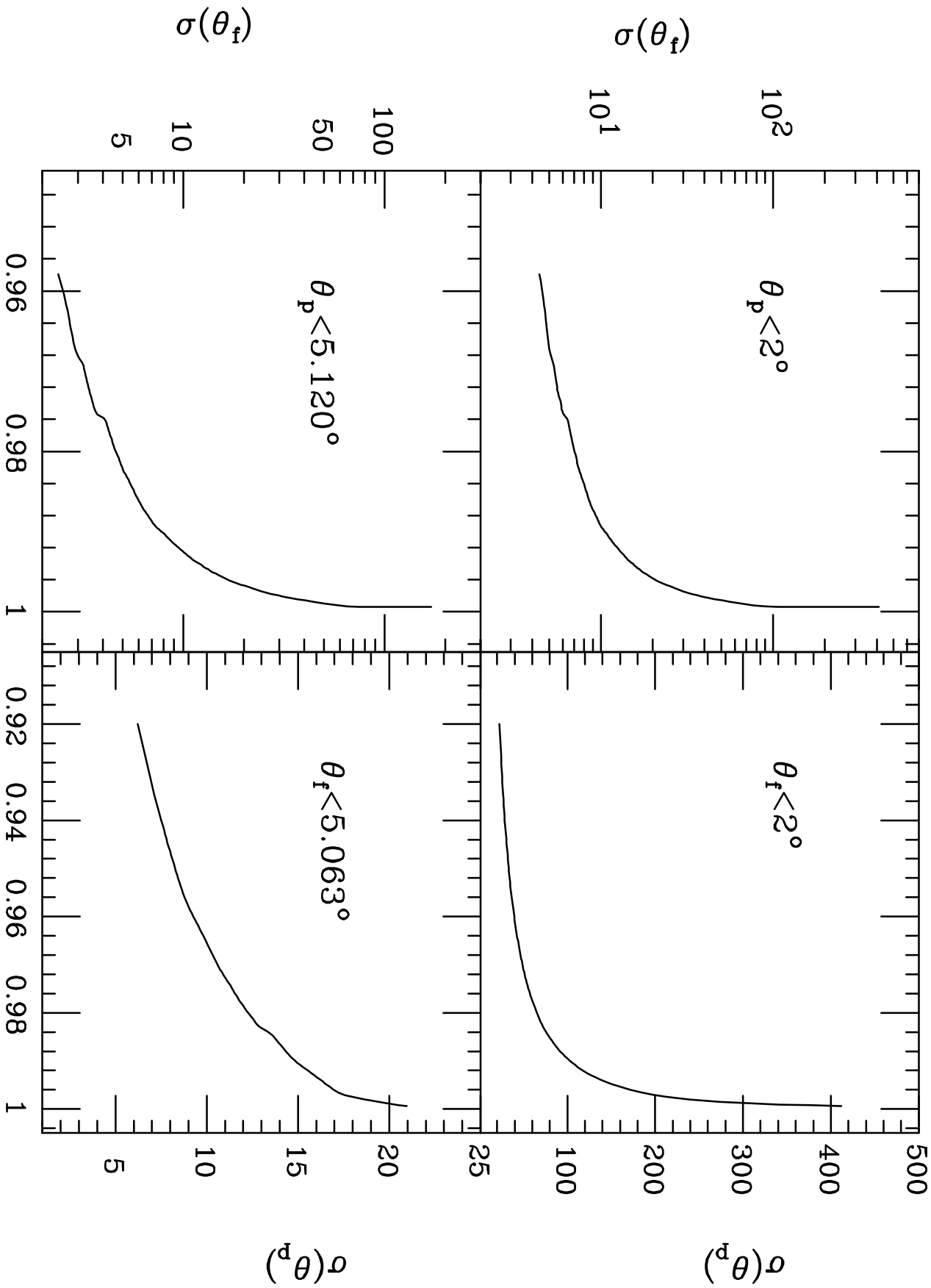


Fig. 6